 doi:10.20944/preprints202210.0298.v1

Article

Backstepping Control Design in Conjunction with an EKF-based Sensorless Field-Oriented Control of an IPMSM

Caglar Uyulan[1]

[1]İzmir Katip Çelebi University, Faculty of Engineering and Architecture, Department of Mechanical Engineering, İzmir, Turkey
ORCID and email: 0000-0002-6423-6720 / caglar.uyulan@ikcu.edu.tr

Abstract: The collector and brushless electronic commutation machines based on the working principle of the direct current machines have been widely used in industrial applications through the help of the developments in power electronics, microelectronics, permanent magnets, microprocessors&control, digital signal processing technologies, etc. Internal permanent magnet synchronous motors (IPMSMs) are used in increasing numbers due to their advantages such as high torque/current and torque/inertia, robust construction, high efficiency, reliability, etc. The problems brought by position sensors, especially in terms of application, performance, mass production, and cost, have made sensorless control a necessity in drive systems and applications.This paper presents a backstepping control method for speed sensorless IPMSM based on an extended Kalman filter (EKF). First, a comprehensive nonlinear dynamical model of the IPMSM in the direct and quadrature ($d-q$) rotor frame is derived and its state-space representation is obtained. Then, the rotor speed and current tracking backstepping controllers are designed to achieve precise tracking and anti-disturbance performance. The designed controllers are embedded into the field-oriented control (FOC) scheme. The asymptotic stability condition for the backstepping controller is guaranteed through the Lyapunov stability theorem. Finally, An EKF is designed for estimating the immeasurable mechanical parameters of IPMSM and tracking the system states in a finite time with high steady-state precision. The effectiveness of the proposed methodology is proved by conducting simulations having various dynamic operating conditions such as sudden torque load change, command speed change, and parameter variation.

Keywords: Sensorless FOC; IPMSM; backstepping control; EKF

1. Introduction

Permanent magnet synchronous motors (PMSMs) are electrical machines that perform energy conversion with the torque induced as a result of the interaction of the magnetic field caused by the stator currents and the magnetic field of the permanent magnets placed on the rotor. In brushed DC machines, one-way uniform torque is provided by varying the rotor current by the collector. In PMSMs, on the other hand, in every pole change of the magnet in the rotor, the current directions flowing through the windings in the stator are changed by the power electronic switches in the inverter. Thus, an electronically commutated electric machine without a collector and brush assembly is obtained. Permanent magnet motors can be classified as trapezoidal (square wave excitation) and sinusoidal (sine wave excitation) depending on the shape of the voltage induced in their windings. A sinusoidal brushless direct current motor is also known as PMSM [Devgan, 1998; Hughes, 2006].

Free-excited direct current motors have remained unrivaled for a long time in the variable speed control systems class, which are widely used in the industry, due to their easy speed control and linear control structure. This is because the current components that make up the flux and the torque can be controlled independently of each other. In this way, when the flux is kept constant, the torque can be controlled linearly with the

 doi:10.20944/preprints202210.0298.v1

current component that creates it. Changing the excitation current makes the torque response of the motor slow, but changing the armature current makes the torque response of the motor fast. Therefore, armature current is used to control the torque taken from the motor shaft. The excitation current control, on the other hand, is controlled to go higher than the rated speed. However, the brush commutator structure, which is the biggest disadvantage of these machines, caused the machine to require maintenance at certain intervals and not to be used in flammable and dusty environments. Considering all these disadvantages, variable speed drive systems are used in alternating current machines such as asynchronous motors and PMSMs, which do not have a brush commutator structure instead of a direct current machine. Synchronous motors are double-excited machines that always rotate at a synchronous speed depending on the frequency of the source and the number of poles of the motor. The stators of these motors are fed with alternating current and the rotors with direct current. However, in synchronous motors, when the rotor magnetic field is provided with permanent magnets placed on the rotor, the need for a second source is eliminated and PMSMs are obtained. Instead of brush and collector assembly, electronic drivers are used to provide commutation. The position sensors enable the driver to feed appropriate windings. Since there is no current in the rotor of the motor, there are no rotor copper losses. In addition, the disappearance of the magnetizing current increases the power coefficient of the motor. Therefore, it is possible to design these motors with the same power but smaller dimensions and higher efficiency than other motors. Excitation with a permanent magnet has provided great advantages to the synchronous motor [Gra˘dinaru 2012; Engelmann&Middendorf, 1995]. If these advantages are listed:

- The stator current is only used to generate torque. Since the current has no magnetization component, its efficiency is higher than an induction motor of the same power;
- They do not require periodic maintenance as there are no brushes and rings. Efficiency is higher as there is no heat loss in the rotor. In addition, they are quieter as there is no noise from the brush and collector;
- Excitation with a permanent magnet brings flexibility to motor design;
- Rotor size is reduced due to the lack of winding, therefore it has a higher torque/inertia ratio and power ratio. Thus, it is preferred to be used in applications requiring high performance such as robotics and space applications [Louis, 2011].

The $d-q$ axis model can also be applied to PMSM, allowing the motor to be controlled like a DC motor, making PMSM motors a powerful alternative to a DC motor. For ideal smooth and vibration-free continuous torque generation, the voltage and current excitation must be purely sinusoidal. In this type of motor, the stator windings around the air gap are sinusoidally distributed and the magnetic flux density produced by the magnets placed in the rotor changes along the air gap [De Soricellis&Rapp, 2019]. The rotor angular position at each time t synchronizes with the supplied stator sinusoidal phase currents. PMSMs are fed through a current-controlled inverter with the help of current sensors placed on each phase and a high-sensitivity position sensor. Any disturbance that can cause phase currents or induced voltage to diverge from the sinusoidal waveform will produce unwanted torque vibration components in these motors. Therefore, high-sensitivity optical encoders or angle detectors (resolvers) are used for position detection. The use of this type of sensor causes an increase in system cost and complexity of control [Gamazo-Real et al., 2010; Sain et al.,2021].

PMSMs can be divided into surface magnets machines and internal magnets machines. Surface magnet machines have a small rotor radius and low inertia torque. Since the magnetic permeability of magnets is almost the same as that of air, the effective air gap is the sum of the actual air gap and the thickness of the magnets. Surface magnet machines do not create reluctance torque due to the d-and q-axis inductances being equal. They have easy demagnetization caused by the armature reaction of magnets and are not suitable for field weakening. Internal magnet motors have a strong mechanical

 doi:10.20944/preprints202210.0298.v1

structure as the magnets are placed inside the rotor. PMSMs with internal magnet structures can produce higher torque per unit volume due to the torque component of the magnet and armature current. At the same time, reluctance torque is also produced due to the different inductances in the d-and q-axis. The reluctance torque can be controlled by the number, thickness, and location of the rotor flux barriers. The reason why this type of machine is widely used in industrial applications as an ideal electrical machine is that it has many features such as high efficiency, small volume, small weight, reluctance torque, and field weakening in a large area. In the internal magnet structure, the effective air gap is small and the demagnetization of the magnets is difficult [Laskaris&Kladas, 2008; Wu et al.,2022]. In PMSMs, the constant power-speed range depends on the permanent magnet rotor structure, and the optimization of the rotor can improve the constant power-speed range. Magnets can be placed on the rotor superficially, on the inner surface of the rotor, on the rotor in the form of rods, in the form of single and multiple barriers, axial laminated, segmented, V-shaped, or W-shaped, respectively. They provide extremely high inductance values and increase the field weakening capability [Yamakawa et al., 2005; Bernard et al., 2015].

Many methods have been developed to obtain rotor position and speed from electrical quantities, eliminating the need for sensors. These methods generally rely on manipulating motor equations such that rotor position and speed are a function of terminal values. The basic principle of sensorless control in PMSMs is that the position information is obtained from:

- the terminal and induced voltage in the motor depending on the rotor speed and position;
- the motor parameters;
- the calculation of the inductance by monitoring the current in real time;
- the injection of a high-frequency&low-energy signal to the stator windings;
- detecting the two-phase current and converting their absolute values into direct current (DC) information;
- extracting it from model reference adaptive systems;
- observer-based techniques or flux estimation algorithms, etc [Brando et al., 2017; Haque&Rahman, 2009; Shibano&Kubota, 2009; Yoon-Ho Kim&Yoon-Sang Kook, 1999].

Sensorless control methods in PMSMs can be broadly divided into three groups: Model-based state predictors (adaptive and non-adaptive methods), saliency&signal injection-based methods, and artificial intelligence algorithms.

Each method has its advantages and disadvantages. The features showing the superiority of the applied sensorless position and velocity estimation method can be listed as steady-state error, dynamic behavior, noise sensitivity, low-speed operation, parameter sensitivity, simplicity, fast response, and calculation time.

Current model-based estimation algorithms are widely used in industry and especially in-home appliance applications, as they are easy to implement and resistant to load torque variation. Position estimation is made with the d-and q-axis current errors between the actual model and the predictor model. The accuracy of the motor model parameters is very important in this method [Park et al., 2010; Zhang et al., 2021].

In non-adaptive methods, estimation algorithms that monitor stator voltages and currents are used. The most important features of these methods are computational ease, uncomplicated observer requirement, and fast response without delay. However, high-accuracy motor parameters are required and the sensitivity of the parameters to noise causes calculation errors [Wang et al., 2019; Benjak&Gerling, 2010a, Benjak&Gerling, 2010b].

In flux estimation algorithms, the flux is estimated from the voltage and current information obtained by measurement, and position estimation is made with the help of a quadratic polynomial-based curve created by using this. To perform sensorless control,

 doi:10.20944/preprints202210.0298.v1

the motor must be started at a previously known position. Therefore, obtaining the initial position information of the rotor is important for estimation. Integration errors at low speeds, long computation time, sensitivity to parameter changes, and needing an expensive signal processor for solving complex algorithms are the main problems. There are studies to determine the rotor position from near zero to full speed in terms of a function of the measured currents and calculated voltages [Krishnan, 2017; Kim&Ehsani, 2004; Kim et al., 2007].

There are other studies based on flux estimation algorithms in the literature. Active flux monitors make position estimations by converting any PMSM into a salient pole machine. The active flux accepts the existence of an imaginary flux that creates the reluctance torque caused by the saliency in the rotor structure, and adds this flux as an imaginary part to the flux of the magnets, revealing an expanded flux. Therefore, it can also be interpreted as a torque-producing flux in salient pole machines. In addition, this flux is aligned to the transverse axis. Thus, the rotor position and speed monitor become more suitable for wide speed ranges and make smaller dynamic errors [Boldea&Agarlita, 2011; Toso et al., 2018]. In another study, "active flux" observer and space vector modulation direct torque and flux control were performed for an IPMSM in a wide speed range without using a motion sensor and signal injection [Boldea et al., 2009]. A longitudinal axis reactance function is given, in which magnetic saturation is also taken into account. Since the effective flux position and rotor position are identical, a noticeable simplification has been achieved in rotor position and velocity estimation. Even higher speeds are possible with field weakening. In another study, a sensorless speed estimation algorithm based on flux and instantaneous reactive power was designed and analyzed using vector control. Measurement errors in motor parameters, line currents, and input voltages cause errors in speed estimation [Sagar&Joseph, 2013]. These errors can be compensated with instantaneous reactive flux. The estimation method based on instantaneous flux provides higher performance by avoiding the thermal drift problem compared to the flux estimation method. The flux-dependent speed estimation method depends on the current and velocity relationship in the $\alpha - \beta$ axes. The velocity estimate, which depends on the instantaneous reactive power, is extracted from the voltage equations because the velocity information is contained within the induced motion voltage. Algorithms are tested in simulations using a space vector pulse width modulated inverter. This estimation method is less responsive to noise, obtains stable information from stator currents and voltages, and provides higher performance. Sensorless control methods based on the measurement of the motion voltage induced in the motor are the easiest, and most widely used and many kinds of research have been done. The sensed EMFs are used in various ways to determine the appropriate switching sequences for the power switch elements in the inverter. The main disadvantage of this method is that the sensing process cannot be performed correctly due to the low induced voltage at the start-up and especially at low speeds. This situation results in the need for an additional take-off method to apply this method. Therefore, techniques based on this method have problems in take-off and transient operation and can be used in a narrow speed range. The need for an artificial neutral point, voltage divider, and filter are the downsides of these methods. Especially at low speeds, position estimation is very sensitive to stator resistance. By using the third harmonic component in the voltage induced in the non-powered phase in PMSMs, sensorless control algorithms have also been developed, including the field weakening region. This method achieves good starting performance, a high torque/current ratio, and high efficiency over a wide speed and load range. The main disadvantage of the method is that the amplitude of the third harmonic component is too small to be detected at low speeds. In addition, the need for an additional circuit and position errors in integration at low speeds are other problems [Shen et al., 2003; Song et al., 2021; Tanaka&Miki, 2007].

Induced motion voltage-based methods estimate the motor with a frequency that is equal to the fundamental electrical frequency proportional to the rotational speed of the rotor. In the basic analytical torque equations of the motor, current and speed are included

 doi:10.20944/preprints202210.0298.v1

as state variables and these equations are not linear. Since the speed and position information of the motor are non-linear, a non-linear observer is needed to perceive them. The first proposed methods are proposed for surface magnet machines. As it is known, machines with surface magnets do not have protrusions, so position and velocity information can only be determined by the induced motion voltage. However, both the position information and the phase inductance information of internal magnet synchronous motors change depending on the saliency. Saliency can be defined as the change in phase inductances depending on the position. In salient pole synchronous motors, the inductances of the direct and quadrature axis are different from each other. By combining the induced motion voltage estimator and the current-based model of the PMSM, the control and position detection problems that are problematic at low speeds are eliminated [Jung-Hyo Lee et al.,2008].

Although accurate induced motion voltage estimation is available, control is limited in low-speed regions. Since the induced motion voltage constant varies according to various loads and speeds, it cannot make an accurate prediction. On the other hand, the model-based sensorless method is quite durable for controlling torque over a wide range of PMSM. The estimation method based on the measurement of phase currents and voltages and the motor model in position and velocity estimation provides significantly accurate estimation by removing position errors [Aite Driss&Yousfi, 2013]. To improve the dynamic performance of traditional induced motion voltage and position sensing methods, the phase-locked loop (PLL) that causes unbalance in the system is eliminated [Honglin Zhou et al., 2012]. Instead of directly filtering the fast-changing rotor position signal, it calculates the starting position with high accuracy by filtering the slowly changing signals. In adaptive methods, the estimated output information is produced by using the input sizes measured from the real system in the mathematical model of the machine. The error between the measured quantities and the estimated output information is used as feedback in the system model to validate the predicted quantities. The biggest advantage of using an observer is that all state variables in the system model can be predicted. Downsides are controlled at low speeds, complex algorithms, and over computation [Benjak&Gerling, 2010].

Since the PMSM model has a nonlinear structure, it is appropriate to use the extended Luenberger observer (ELO) for position and speed estimation. Accordingly, the nonlinear system model is linearized at each sampling time with the help of the Jacobian matrix. Studies have been carried out using the extended Luenberger observer for state estimation in alternating current drivers [Elmas&Zelaya-De La Parra, 1996; Aydeniz&Şenol, 2011]. Another adaptive method is model-based adaptive control (MRAC). The speed and position estimation methods used can be classified in various ways according to the state variables. The most commonly used ones are rotor flux-based, reverse emf-based, and stator current-based, respectively [Yousfi et al., 2009; Jiaxi et al., 2007; Zhao et al., 2013]. The extended induced voltage is used as the new state variable in the adaptive velocity observer [Zhiqian Chen et al., 2003]. Extended induced voltage; includes the induced action voltage and the change in phase inductances. When the motor equations are rewritten in terms of extended induced motion voltage, only the position-dependent terms remain in the equation. The position of the internal magnet synchronous motor is estimated with the expanded induced voltage error observer according to the stator and rotor reference system [Ichikawa et al., 2001]. In another study, a simplified mathematical model of a PMSM and MRAC based on a voltage and current model was used to estimate speed [Medagam et al., 2009]. The model has been developed to minimize the effects of MRAC parameter uncertainties and increases the estimation performance. According to the experimental results, much more sensitivity resulted in good speed response and performance at low and high speeds. PMSM is controlled by a field-oriented control (FOC) method [Asri et al., 2011; Wei-Hua Li et al., 2012]. A model reference adaptive system (MRAS) was used to eliminate the speed sensor. The performance of the proposed method has been tested under balanced and unbalanced motor operating conditions. Among the

 doi:10.20944/preprints202210.0298.v1

observer-based prediction algorithms, systems with Luenberger observers generally have better performance than MRAS-based systems. MRAS has a higher error in predicted values. Also, the Luenberger approach has fewer memory requirements and computation time. In another study, an extended Kalman filter (EKF) is aimed to minimize the problems caused by parameter error. This observer method is more independent against parameter changes and is widely used in nonlinear systems due to its optimality, ease of processing, and durability [Merzoug, 2011; Janiszewski, 2010]. With the developments in digital signal processing, the computation time load of the EKF is easily overcome. Algorithms can be implemented quickly with an inexpensive DSP motor controller [Aishwarya&Jayanand, 2016; Qiu, 2021]. Since parameter errors and noises in the measurement are taken into account in the structure of the method, the EKF method is very resistant to parameter errors and noises. Since initial position information is not needed for take-off, the motor can be started from any unknown initial position [Bolognani et al., 1999; Vyncke et al., 2010; Benchabane et al., 2010; Comnac et al., 2002]. Unexpected balance points can also be moved with appropriate compensation from the observer. Real-time EKF calculations are performed on a sensorless PMSM driver with a floating-point DSP that performs current and speed control loops and space vector pulse width modulation (SVPWM) [Bolognani et al., 1999]. The EKF estimation algorithm used in the study does not need the initial rotor position and mechanical parameters, eliminating the deficiencies of other estimation techniques and reducing the parameter sensitivity. In addition, the load torque was taken as the state variable, so that the load torque did not represent an unknown disturbance effect in the system. In signal injection-based methods, the inductance change in PMSM is used according to the rotor position. A high-frequency voltage or current is injected into the fundamental component and rotor position information is obtained from current harmonics with signal processing. Position information can be obtained at take-off and low speeds, and it is resistant to parameter changes. Therefore, it has advantages over other techniques. It can be classified as a rotating injection method and pulsating injection method according to the direction of the injected signal. There are methods in the literature based on PWM-excited signal processing without signal injection [Corley&Lorenz, 1998; Dobrucky et al., 2006]. Estimated position information is obtained by injecting a high-frequency signal into the system, which operates in a wide range from stationary to high-speed states. The main important benefit of this study is; It is an easily applicable estimation method in a wide range from high-speed to zero-speed situations. The estimation of the rotor position was determined by applying a high-frequency current signal to the stator windings. In addition, an adaptable PMSM model was used in this study, and the variation of machine parameters was also taken into account [Shanshan et al., 2007; Xiao et al., 2010]. Two different sensorless vector control methods were investigated for PMSM-driven in the low-speed range. Various experiments were carried out by adding high and low-frequency signals to the system. According to the experimental results, both methods can be configured simply and are suitable for efficient operation. Although better dynamic performance is obtained in the high-frequency signal addition method, the noise is very high. The methods using the magnetic saliency effect are very complex to implement in real-time and it is very difficult to apply to machines with different structures and features. However, they perform quite well at low speeds and can also be positioned at take-off [Wang et al., 2010; Yan&Zhu, 2006; Anping&Jian, 2010]. A non-linear PMSM model is considered and the rotor position is determined using the saliency effect. The offsets reflect the changes in the stator winding inductance depending on the rotor position and the stator phase current. The non-linear inductance of the PMSM was measured at various rotor positions and stator currents. Rotor position and stator current equations are explained using the Fourier series. As a result of the simulations made in low and high-speed regions, this method was not found suitable for operation in low-speed regions [De Belie et al., 2010].

Artificial neural networks (ANNs), fuzzy logic algorithms, and ANFIS are artificial intelligence methods used in the sensorless control of PMSMs. The complexity that can be

Preprints (www.preprints.org) | NOT PEER-REVIEWED | Posted: 20 October 2022 doi:10.20944/preprints202210.0298.v1

experienced in the selection of the network structure and the calculation of the control algorithm, the trial and error system in the structure of the ANN makes the applicability of the sensorless control difficult while weakening the durability and increasing the error rate [Chaoui et al., 2009; Daya&Subbiah, 2010; Butt et al.,2003]. A high-frequency low voltage was applied to the stator to determine the initial rotor position using the artificial neural network. The currents flowing through the stator phases and the rotor position at that moment were recorded by applying voltages. The operations were repeated for different rotor positions and the learning set was created for the artificial neural network. In the operating state, the motor is first fed with test voltages and the measured currents are applied to the ANNs, and the instantaneous initial rotor position for the motor is determined. After the experiment, it was observed that the position error was at the minimum level [Urbanski&Janiszewski, 2021].

Since it is aimed to use a robust sensorless control algorithm in a wide range along the low and high speed and variable load profile; the backstepping control algorithm based on EKF, which has advantages in this direction in terms of computation and accuracy, was utilized in this study. The rest of this paper is organized as follows. In Sections 2 and 3, the mathematical model and the FOC-based backstepping controller for IPMSM are presented. The speed and position information of IPMSM is estimated by the EKF observer in Section 4. Section 5 presents simulation examples to demonstrate the effectiveness of the proposed method. Finally, some conclusions are presented in Section 6.

2. The mathematical model of IPMSM

In this section, the dynamic model required for the analysis and control of the IPMSM is built. The structure and equivalent circuit of a two-pole, three-phase star-connected PMSM are shown in Fig.1.

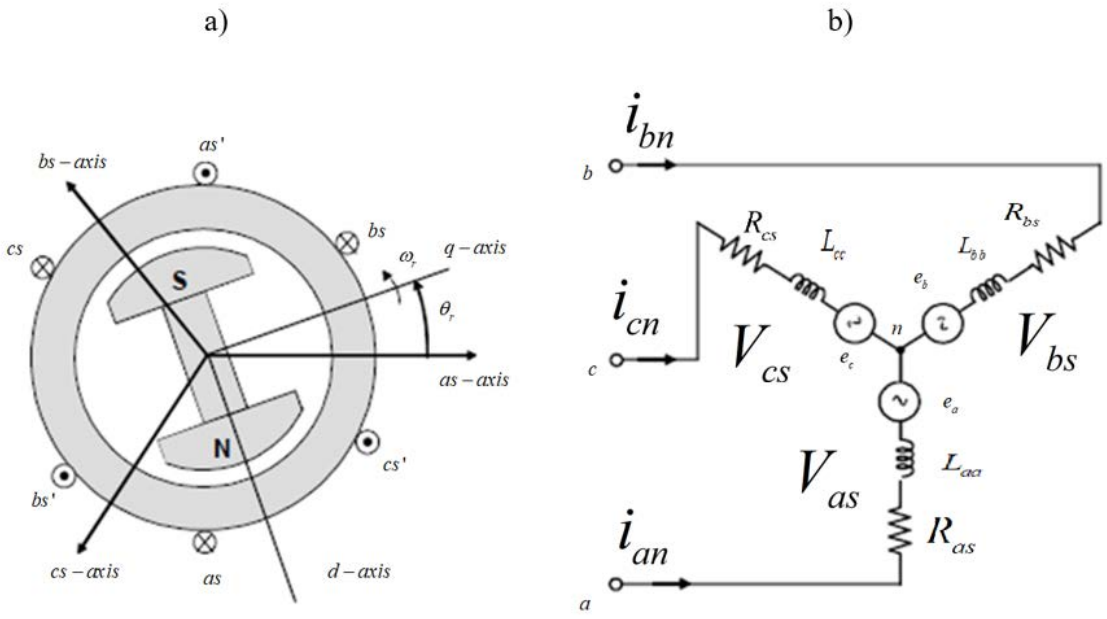

Figure 1. a) structure and b) equivalent circuit of IPMSM.

According to Fig.1, the stator voltage equations of the machine can be written as in Eq.1

$$\boldsymbol{v}_{abcs} = \boldsymbol{R}_s \boldsymbol{i}_{abcs} + \frac{d\boldsymbol{\psi}_{abcs}}{dt}$$
$$\boldsymbol{R}_s = diag[R_s \quad R_s \quad R_s]$$
$$\boldsymbol{\psi}_{abcs} = \boldsymbol{L}_s \boldsymbol{i}_{abcs} + \boldsymbol{\psi}_m$$

Preprints (www.preprints.org) | NOT PEER-REVIEWED | Posted: 20 October 2022 doi:10.20944/preprints202210.0298.v1

$$\boldsymbol{\psi}_m = \psi_m \begin{bmatrix} \sin(\theta_e) \\ \sin\left(\theta_e - \frac{2\pi}{3}\right) \\ \sin\left(\theta_e - \frac{4\pi}{3}\right) \end{bmatrix} \quad (1)$$

where $\boldsymbol{v}_{abcs}$ stator voltages, $\boldsymbol{i}_{abcs}$ stator currents, $\boldsymbol{R}_s$ stator winding resistance matrix, $\boldsymbol{L}_s$ stator inductance matrix, $\boldsymbol{\psi}_{abcs}$ stator fluxes, $\boldsymbol{\psi}_m$ rotor flux provided by permanent magnets, θ_e rotor electrical position, respectively.

Since the inductance matrix $\boldsymbol{L}_s$ given in the model is a function of the rotor's electrical position θ_e and must be differentiated within the model, the current model of IPMSM is quite complex. Various axes transformations can be made to free the inductance matrix from dependence on the rotor position, facilitate the analysis of the machine model, and simplify the control algorithms. Clarke transform is utilized to reduce three-phase quantities in the fixed plane to two phases perpendicular to each other. These two phases are called α and β. Likewise, two-phase quantities that are also in the fixed plane and differ by $90°$ between them can be converted to three-phase quantities in the fixed plane. This time the transformation is called the inverse Clarke transform. The Clarke transform takes place in the fixed plane. However, as will be mentioned frequently in control, it is also necessary to switch from a fixed plane to a rotating plane or from a rotating plane to a fixed plane. This transformation is possible by using the Park transformation. In this plane, the phases are called d and q. The inverse of the Park transformation is also possible, which means a transition from a two-phase moving plane rotating with speed θ to a two-phase fixed plane. Modeling the PMSM in the $d-q$ axis set in Fig.1a provides great convenience in the control algorithm. Since these axes are fixed to the rotor axis, it is also called rotor-referenced axes. The d axis is in the direction of rotor flux and the q axis is 90^o perpendicular to the d axis. In electrical machine models, voltage, current, and flux transformation matrices, which are vector quantities in axis set transformations, are transformed as in Eq.2.

$$\boldsymbol{f}_{qd0s} = \boldsymbol{K}_s \boldsymbol{f}_{abcs} \quad (2)$$

where $\boldsymbol{K}_s$ is the transformation matrix, $\boldsymbol{f}_{abcs}$ is equal to $[f_{as} \quad f_{bs} \quad f_{cs}]^T$

To switch from the stator $a-b-c$ axis set to the rotor dq axis set, first the Clarke transformation and then the Park transform is applied. Accordingly, $\boldsymbol{K}_s$ matrix to be used for the transformation will be as follows in Eq.3

$$\boldsymbol{K}_s = \frac{2}{3} \begin{bmatrix} \cos(\theta_e) & \cos\left(\theta_e - \frac{2\pi}{3}\right) & \cos\left(\theta_e - \frac{4\pi}{3}\right) \\ \sin(\theta_e) & \sin\left(\theta_e - \frac{2\pi}{3}\right) & \sin\left(\theta_e - \frac{4\pi}{3}\right) \\ \frac{1}{2} & \frac{1}{2} & \frac{1}{2} \end{bmatrix} \quad (3)$$

Accordingly, if $\boldsymbol{v}_{abcs}$, $\boldsymbol{i}_{abcs}$, and $\boldsymbol{\psi}_{abcs}$ are converted to the quantities in the $d-q$ axis according to Eq.2 with the transformation matrix given in Eq.3, the flux and voltage equations regarding the mathematical model of the IPMSM in the rotor reference system ($d-q$ axis) are written as follows in Eq.4.

$$V_{ds} = R_s i_{ds} + \frac{d\psi_{ds}}{dt} - \omega_e \psi_{qs}$$
$$V_{qs} = R_s i_{qs} + \frac{d\psi_{qs}}{dt} + \omega_e \psi_{ds}$$
$$\psi_{ds} = L_d i_{ds} + \psi_m$$
$$\psi_{qs} = L_q i_{qs}$$
$$\frac{di_{ds}}{dt} = -\frac{R_s}{L_d} i_{ds} + \frac{L_q}{L_d} \omega_e i_{qs} + \frac{1}{L_d} v_{ds}$$
$$\frac{di_{qs}}{dt} = -\frac{R_s}{L_q} i_{qs} - \frac{L_d}{L_q} \omega_e i_{ds} - \frac{1}{L_q} \omega_e \psi_m + \frac{1}{L_q} v_{qs}$$
$$T_e = \frac{3}{2} p\left[\psi_m i_{qs} + (L_d - L_q) i_{ds} i_{qs}\right]$$
$$\omega_e = \mathrm{p}\omega_\mathrm{m}$$
$$\frac{\mathrm{d}\omega_\mathrm{m}}{\mathrm{dt}} = \frac{1}{J}\mathrm{T_e} - \frac{1}{J}\mathrm{T_L} - \frac{\mathrm{B}}{J}\omega_\mathrm{m} \quad (4)$$

Preprints (www.preprints.org) | NOT PEER-REVIEWED | Posted: 20 October 2022 doi:10.20944/preprints202210.0298.v1

$$\frac{d\theta_e}{dt} = \omega_e = p\omega_m$$
$$P = \frac{3}{2}\mathrm{R_s}\left(\mathrm{i_{ds}^2} + \frac{4\mathrm{T_e^2}}{9p^2[\psi_m+(\mathrm{L_d}-\mathrm{L_q})\mathrm{i}_{ds}]^2}\right) \quad (4)$$

where p is the number of pole pairs; R_s is the stator winding resistance; ω_e is the electrical angular frequency; ω_m is the mechanical angular frequency; $V_{ds}, V_{qs}, i_{ds}, i_{qs}$ are stator winding voltage and currents projected into the $d-q$ axis, respectively; ψ_{ds}, ψ_{qs} are stator flux projected into the $d-q$ axis; ψ_m is the rotor flux linkage, L_d and L_q are the stator inductances reflected into the $d-q$ axis; T_e is the motor's electrical torque; T_L is the load torque; J is the rotor inertia; B is the viscous friction coefficient; P is the electrical power.

To formulate the design problem, according to Eq.4, the state-space model of the IP-MSM is constructed as the following nonlinear system in Eq.5

$$\overbrace{\begin{bmatrix}\dot{x}_1\\ \dot{x}_2\\ \dot{x}_3\end{bmatrix}}^{\dot{x}(t)} = \begin{bmatrix}-\frac{B}{J} & \frac{3p\psi_m}{2J} & 0\\ -\frac{p\psi_m}{L_q} & -\frac{R_s}{L_q} & -px_1\\ 0 & px_1 & -\frac{R_s}{L_d}\end{bmatrix}\overbrace{\begin{bmatrix}x_1\\ x_2\\ x_3\end{bmatrix}}^{x(t)} + \begin{bmatrix}-\frac{T_L}{J}\\ \frac{V_{qs}}{L_q}\\ \frac{V_{ds}}{L_d}\end{bmatrix} \quad (5)$$

where $x(t)$ is the state vector. x_1, x_2, x_3 correspond to the ω_m $(rotor\ speed)$, i_{qs} $(stator\ quadrature\ current)$, $i_{ds}(stator\ direct\ current)$, respectively.

The main control objective is confining all closed-loop signals bounded and satisfying global asymptotic convergence of the speed and current tracking errors to zero.

3. Controller Design

3.1. Backstepping Controller Design

Backstepping control is an efficient nonlinear control system method, whose first step is to define a virtual control state. Then, the state is forced to be a stabilizing function. The control input is designed considering Lyapunov stability so that the error variable is stabilized [Iqbal&Memon, 2019; Lin et al., 2017; Rkhissi-Kammoun et al., 2015].

3.1.1. Speed controller

The controller for the speed state x_1 is designed to achieve speed tracking problems, therefore the state tracking error variable is defined as in Eq.6

$$e_1 = x_1^* - x_1 \quad (6)$$

where x_1^* is the reference rotor speed.

To stabilize the speed component, the speed tracking error dynamics are derived using Eq.5 and Eq.6 as in Eq.7

$$\dot{e}_1 = \dot{x}_1^* - \dot{x}_1 = \frac{T_L}{J} + \frac{B}{J}x_1 - \frac{3p\psi_m}{2J}x_2 \quad (7)$$

The following Lyapunov function candidate is chosen as in Eq.8

$$V_1 = \frac{1}{2}e_1^2 \quad (8)$$

The time derivative of the Lyapunov function is expressed as in Eq.9

$$\dot{V}_1 = e_1\dot{e}_1 = \frac{e_1}{J}\left(Bx_1 + T_L - \frac{3p\psi_m}{2}x_2\right) \quad (9)$$

By utilizing Lypunov's stability definition ($\dot{V}_1 \prec 0$), to make the tracking error convergence to zero, Eq.10 must be satisfied

Preprints (www.preprints.org) | NOT PEER-REVIEWED | Posted: 20 October 2022 doi:10.20944/preprints202210.0298.v1

$$\frac{e_1}{J}\left(Bx_1+T_L-\frac{3p\psi_m}{2}x_2\right)=-k_0e_1^2, k_0\succ 0 \tag{10}$$

The backstepping methodology dictates that the virtual control variable input x_2 is found by solving Eq.10 for x_2 as in Eq.11.

$$x_2^*=\frac{2}{3p\psi_m}\left(Bx_1+T_L+k_0Je_1\right) \tag{11}$$

If Eq.11 is satisfied, the speed error approaches zero, i.e., global asymptotic tracking of speed is guaranteed.

Decoupling nonlinear control is utilized in the IPMSM control system. The exact thrust force that drives the motor is obtained by the stator quadrature current (x_2). When the stator direct current (x_3) is forced to drive zero, the coupling term x_1, x_3 in Eq.4 is eliminated and power consumption is minimized in terms of control action.

When $i_{ds}=x_3=0$, the control scheme should be $x_3^*=0$.

3.1.2. Current controller

To satisfy the q-axis current tracking e_2 is chosen as a new state variable given in Eq.12

$$e_2=x_2^*-x_2 \tag{12}$$

The derivative of the e_2 is evaluated as in Eq.13

$$\begin{aligned}\dot{e}_2&=\dot{x}_2^*-\dot{x}_2=\frac{2}{3p\psi_m}\left(B\dot{x}_1+\dot{T}_L+k_0J\dot{e}_1\right)+\frac{R_s}{L_q}x_2+px_1x_3+\frac{p\psi_m}{L_q}x_1-\frac{v_{qs}}{L_q}\\&=\frac{Bx_2}{J}-k_0x_2-\frac{v_{qs}}{L_q}+\frac{R_sx_2}{L_s}+px_1x_3+\frac{2\dot{T}_Lk_0}{3p\psi_m}+\frac{2T_Lk_0}{3p\psi_m}+\frac{p\psi_mx_1}{L_s}-\frac{2B^2x_1}{3Jp\psi_m}-\frac{2BT_L}{3Jp\psi_m}+\frac{2Bk_0x_1}{3p\psi_m}\end{aligned} \tag{13}$$

For the new system based on e_1 and e_2, the second Lyapunov function is defined as in Eq.14

$$V_2=V_1+\frac{1}{2}e_2^2 \tag{14}$$

The time derivative of V_2 is given as in Eq.15

$$\begin{aligned}\dot{V}_2&=e_1\dot{e}_1+e_2\dot{e}_2=e_1\left(\frac{T_L}{J}+\frac{B}{J}x_1-\frac{3p\psi_m}{2J}x_2\right)\\&+e_2\left(\frac{Bx_2}{J}-k_0x_2-\frac{v_{qs}}{L_q}+\frac{R_sx_2}{L_s}+px_1x_3+\frac{2\dot{T}_Lk_0}{3p\psi_m}+\frac{2T_Lk_0}{3p\psi_m}+\frac{p\psi_mx_1}{L_s}-\frac{2B^2x_1}{3Jp\psi_m}-\frac{2BT_L}{3Jp\psi_m}+\frac{2Bk_0x_1}{3p\psi_m}\right)\end{aligned} \tag{15}$$

By utilizing Lypunov's stability definition ($\dot{V}_2\prec 0$), to make the tracking error convergence to zero, Eq.16 must be satisfied

$$\dot{V}_2=-k_0e_1^2-k_1e_2^2, k_1\succ 0 \tag{16}$$

The stabilizing control law is derived from Eq.16 ($\dot{e}_2=-k_1e_2$) by solving the actual control variable v_{qs} as in Eq.17

$$v_{qs}^*=R_sx_2-L_sk_0x_2+p\psi_mx_1+L_sk_1e_2+\frac{BL_sx_2}{J}+\frac{2L_s\dot{T}_L}{3p\psi_m}+L_spx_1x_3+\frac{2L_sk_0T_L}{3p\psi_m}-\frac{2B^2L_sx_1}{3Jp\psi_m}+\frac{2BL_sk_0x_1}{3p\psi_m}-\frac{2BL_sT_L}{3Jp\psi_m} \tag{17}$$

Similarly, the d-axis current controller can be designed by choosing d-axis current tracking error as a new state variable as in Eq.18

Preprints (www.preprints.org) | NOT PEER-REVIEWED | Posted: 20 October 2022 doi:10.20944/preprints202210.0298.v1

$$e_3 = x_3^* - x_3 \tag{18}$$

Differentiating e_3 concerning time and using the results of Eq.4, Eq.19 is obtained

$$\dot{e}_3 = \frac{R_s x_3}{L_s} - \frac{v_{ds}}{L_s} - p x_1 x_2 \tag{19}$$

For a new system based on three errors, the third Lyapunov function is stated as in Eq.20

$$V_3 = V_2 + \frac{1}{2} e_3^2 \tag{20}$$

Differentiating V_3 for time, Eq.21 is obtained

$$\dot{V}_3 = \dot{V}_2 + e_3 \dot{e}_3 = \dot{V}_2 + e_3 \left(\frac{R_s x_3}{L_s} - \frac{v_{ds}}{L_s} - p x_1 x_2 \right) \tag{21}$$

Eq.21 contains the actual control variable v_{ds}. By utilizing Lypunov's stability definition

($\dot{V}_3 \prec 0$), to make the tracking error converge to zero, Eq.22 must be satisfied

$$\dot{V}_3 = -k_0 e_1^2 - k_1 e_2^2 - k_2 e_3^2, k_2 \succ 0 \tag{22}$$

The stabilizing control law is derived from Eq.22 ($\dot{e}_3 = -k_2 e_3$) by solving the actual control variable v_{ds} as in Eq.23

$$v_{ds}^* = R_s x_3 + L_s k_2 e_3 - L_s p x_1 x_2 \tag{23}$$

The objective of backstepping control for IPMSM is completed.

3.2. Field-Oriented Vector Control

FOC allows for the separation of the magnetizing flux and torque flux components of the stator currents, so it is possible to control the torque independent of magnetization. According to the electromagnetic laws, the torque created in the synchronous machine is equal to the vector product of the magnetic fields existing in the machine as given in Eq.24

$$\boldsymbol{T}_e = \boldsymbol{B}_{stator} \times \boldsymbol{B}_{rotor} \tag{24}$$

A PMSM consists of a permanent magnet rotating in the rotor and symmetrical windings placed in the stator surrounding it. The field vector created by the current flowing through each winding is combined with the field vectors created by the other windings to form the total magnetic field vector ($\boldsymbol{B}_{stator}$). It is possible to create a magnetic field of any direction and amplitude in the air gap by controlling the current flowing in each winding. The torque is produced by the attraction or repulsion between the total stator magnetic field strength and the rotor magnetic field strength. According to Eq.24, in any rotor position, there is a net stator field direction that makes the torque the highest, as well as a direction that makes the torque zero. If a net stator field is produced in the same direction as the field produced by the permanent magnet rotor, no torque is produced. The fields affect each other to produce a force, but since the force is in line with the direction of rotation of the rotor, it does not rotate the motor, it just compresses the bearings. On the other hand, if the stator field is perpendicular to the field produced by the rotor, magnetic forces try to rotate the rotor and the torque is maximized. A stator field chosen in any direction and size can be divided into perpendicular and parallel components of the rotor field. In this case, the perpendicular component produces torque, while the parallel component generates a useless compression force. Therefore, an efficient PMSM driver will increase the perpendicular component of the stator field while decreasing the component parallel to the rotor field. While designing and modeling the control system, current windings are used as control variables instead of stator magnetic field, since magnetic field intensities cannot be measured directly. In PMSM, the stator field vector is produced by

 doi:10.20944/preprints202210.0298.v1

three-phase windings placed at a geometric angle of 120°. There is a 120° phase difference between the field vectors produced by each winding. The net magnetic stator field is produced by the sum of these three components. "Current space vectors" are used to model the fields produced by the stator windings in terms of winding currents. The current space vector of a winding is in the direction of the field vector produced by the winding and its amplitude is proportional to the current flowing through the winding. This allows the total stator field to be represented by a current space vector that is the sum of the current space vector of the three phases. The current space vector is an apparent current flowing through a rotating apparent (imaginary) winding, introduced to relate the direction and amplitude of the real stator field to the current flowing through the stator windings. As in the stator field, the stator current space vector can be divided into components perpendicular and parallel to the axis of the rotor magnet. The longitudinal axis current component generates a magnetic field at appropriate angles to the rotor magnet, which generates torque. The transverse axis current component produces a field parallel to the rotor magnet, which does not produce torque. Because bearing wear causes problems such as heating, transverse axis currents are always set to zero in a good control algorithm. In this case, the moment will be proportional to the amplitude of the current space vector. To efficiently produce a constant uniform torque, the stator current space vector must be of constant magnitude and rotate with the rotor to lie on the longitudinal axis, regardless of rotor position and speed. Although the stator current space vector is of constant magnitude and direction when viewed from the rotating rotor axis, it draws a circle as the motor rotates when viewed from the fixed stator axis. The current space vector is produced by the sum of the vector components of each of the motor windings and each of the three windings is located at a geometric angle of 120°. Motor currents should preferably be sinusoidal and have a phase difference of 120° between them. Sinusoidal winding currents depend on the rotor angle, so the transverse axis component of the stator current space vector is zeroed while the longitudinal axis component is made as high as possible. Vector control is a method that enables these machines to be controlled like a direct current motor by reducing the stator currents of a three-phase alternating current motor to two components perpendicular to each other in variable-speed drive systems. One component creates the flux of the motor, while the other component creates the torque. The current components that make up the reference torque and flux are compared with the currents of the motor reduced to two components. A controller keeps the measured current components constant in the reference current component. According to the output of the PI controller, the semiconductor power elements in the inverter (variable speed drive systems) are switched. Vector control induction motor is used quite often in PMSMs. Thanks to vector control, it is possible to control in a wide speed range. In addition, rated torque at zero speed can be achieved and the dynamic performance of the system can be significantly improved. In FOC, the current and voltages of the motor are controlled at the $d-q$ reference axes of the rotor. It is the mathematical conversion of the measured motor current from the three-phase fixed axis set of the stator windings to the two-axis rotational $d-q$ reference axes before it enters the controller. Similarly, before the voltage applied to the motor is used at the output of the pulse width modulator (PWM), it must be mathematically converted from the $d-q$ reference axes of the rotor to the three-phase reference axes of the stator. These transformations, which are the basis of FOC, usually require DSPs or high-performance processors with fast mathematical processing capability. Indirect field-directed control or vector control has become the standard for AC drives with speed and torque control to achieve high dynamic motor behavior. Torque control of PMSM in constant torque region is done by rotor reference plane quadrature axis (i_{qs}) current. This region is the region up to the motor-rated speed. The constant power region is the region for speeds after the rated speed of the motor. In this region, besides the quadrature axis current of the motor (i_{qs}), the direct axis current (i_{ds}) is also controlled. In vector control methods, the use of phase transformations provides simplicity in motor dynamic equations.

Preprints (www.preprints.org) | NOT PEER-REVIEWED | Posted: 20 October 2022 doi:10.20944/preprints202210.0298.v1

Indirect vector control is summarized below:

Step 1: Two of the three stator phase currents are measured and the third current is determined using Kirchoff's current law ($i_{as} + i_{bs} + i_{cs} = 0$).

Step 2: Three-phase currents are converted from a 3-axis stator system to a 2-axis stator-based coordinate system using Clarke transformation $\left(i_{as}, i_{bs}, i_{cs}\right) \Rightarrow \left(i_{\alpha s}, i_{\beta s}\right)$.

Step 3: The components in the two axes of the stator current are time-dependent and very complex to control with a specific controller. Therefore, it is necessary to reduce it to the reference axis fixed to the rotor. This conversion is done using Park transformation. Instantaneous values of the rotor angle are needed $\left(i_{\alpha s}, i_{\beta s}\right) \Rightarrow \left(i_{ds}, i_{qs}\right)$.

Step 4: The error signals entering the controller are obtained from the difference between the i_{ds} and i_{qs} currents, the reference currents. The rotor magnetizing flux is controlled concerning i_{ds} and the motor output torque is controlled by reference to i_{qs}. The output of the controller will be the voltage vector v_{ds} and v_{qs} to be sent to the motor**.**

Step 5: Since the rotor angle is required for the FOC algorithm, the v_{ds} and v_{qs} output values from the controller are returned to the stationary reference system using the rotor angle, and the $v_{\alpha s}$ and $v_{\beta s}$ values are calculated. When $i_{\alpha s}$ and $i_{\beta s}$ are inputs, the new conversion angle is estimated. Outputs of controllers are converted back to three-phase stator reference by going through reverse Park and reverse Clarke transformations.

Step 6: The voltages $v_{\alpha s}$ and $v_{\beta s}$ are converted to three-phase voltage v_{as}, v_{bs}, and v_{cs} to obtain pulse width modulated signals that will yield the three-phase voltage at the inverter output. The v_{ds} and v_{qs} output values from the controller are returned to the fixed reference system using the new angle value. The PWM space is tuned using vector shifting by generating a three-phase reference signal.

Since the rotor magnetic field always extends along the d-axis of the rotor $d-q$ axis set, the component of the stator field in the d-axis must be zero and the component of the stator field in the q-axis must be maximum. To efficiently produce a constant uniform torque, the stator field (hence the stator current space vector) must be of constant magnitude on the q-axis, and to achieve this, it must rotate with the rotor regardless of rotor position and speed. The flux and torque control algorithm tries to keep the resultant stator magnetic field always on the q −axis of the rotor by adjusting the stator winding voltages and making its d −axis component zero. FOC allows controlling separately the component of the stator magnetic field formed by the stator currents on the q-axis and the torque, and the magnetization with the component on the d-axis. There are two separate current control loops for the q and d components of the stator currents. The block diagram of the speed control of FOC is given in Fig.2.

Since the motor torque is directly dependent on the quadrature current i_{qs}, controlling the i_{qs} means controlling the torque. The output of the speed controller is the reference current i_{qs}. The reference of the i_{ds} current should be zero throughout the operation. The output of the i_{qs} and i_{ds} current controllers are the voltages v_{qs} and v_{ds}, which must be applied to the motor, respectively. As can be seen, in FOC, the current and voltages of the motor are controlled at the $d-q$ reference frame of the rotor. The mathematical conversion of the measured motor current from the three-phase $a-b-c$ axis set of the stator windings, first to the fixed α-β axis set of the stator (Clarke transform), and then to the rotor $d-q$ reference axis set (Park transform), before entering the controller. Similarly, the voltage to be applied to the motor is mathematically converted from the $d-q$ reference axis set of the rotor to α-β (Inverse Park transform) components on the fixed stator axis set before it is used in the PWM. The purpose of the transformation in all these reference axes is to save the time-varying sinusoidal motor current and voltage signals from the dependence of time and to transform them into a direct current signal. In FOC, since the reference currents are constant in the $d-q$ reference frame, the controller operates in DC mode instead of a sinusoidal signal. This isolates the controller from time-depend-

Preprints (www.preprints.org) | NOT PEER-REVIEWED | Posted: 20 October 2022 doi:10.20944/preprints202210.0298.v1

ent current and voltage, thus eliminating the frequency response limitation of the controller and the phase shift on the torque and speed of the motor. The quality of current control becomes independent of the angular speed of the motor and it is possible to control over a wide speed range. In addition, maximum torque control at zero speed can be achieved and the dynamic performance of the system can be significantly improved.

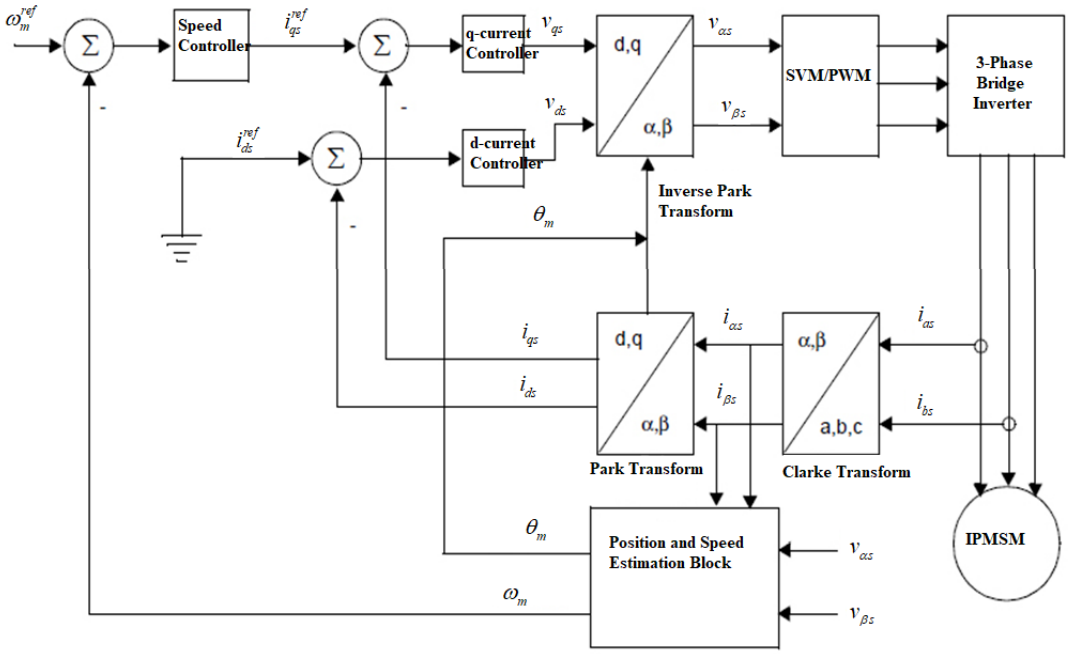

Figure 2. Field-oriented control block diagram of PMSM.

4. Extended Kalman Filter (EKF)

Extended Kalman filter (EKF), which is a stochastic method due to its success in state estimation in non-linear systems, is widely used for estimating rotor position and speed in synchronous motor drives. EKF is an optimal estimator using the least squares method for state estimation in dynamic nonlinear systems [Dhaouadi et al., 1991; Haykin, 2001].

In a non-linear discrete-time system; system noises (w_k) including system disturbances and model uncertainties and the measurement noises (v_k) are represented in Eq.25 with zero-mean white Gaussian noise having covariance matrices Q_k and R_k , respectively,

$$x_k = f\left(x_{k-1}\right) + w_{k-1}$$
$$z_k = h\left(x_k\right) + v_k \qquad (25)$$

Here, $f\left(x_{k-1}\right)$ shows the nonlinear state equations of the system. The initial value of states

(x_0) is a random vector with covariance $P_0 = E\left[\left(x_0 - \mu_0\right)\left(x_0 - \mu_0\right)^T\right]$ and mean value $\mu_0 = E\left[x_0\right]$. The w_k v_k noises are uncorrelated to each other and the initial state vector x_0.

The following relations given in Eq.26 are valid [Kim&Huh, 2011; Mohsin, 2000].

Preprints (www.preprints.org) | NOT PEER-REVIEWED | Posted: 20 October 2022 doi:10.20944/preprints202210.0298.v1

$$
\begin{aligned}
&E\left[w_k\right]=E\left[v_k\right]=0\\
&E\left[w_k {w_k}^T\right]=Q_k\\
&E\left[v_k {v_k}^T\right]=R_k\\
&E\left[w_k {w_j}^T\right]=0,\ k\neq j\\
&E\left[v_k {v_j}^T\right]=0,\ k\neq j\\
&E\left[w_k {x_0}^T\right]=0,\ \forall k\\
&E\left[v_k {x_0}^T\right]=0,\ \forall k\\
&E\left[w_k {v_j}^T\right]=0,\ \forall k\ ve\ \forall j
\end{aligned}
\tag{26}
$$

The algorithm consists of two steps. ***Step 1:*** Predict the next state using the previous state estimation; ***Step 2:*** Update/correct the previous estimate by looking at the measured values.

The pseudocode scheme of the EKF algorithm is given in Table 1 [Dilys et al., 2021; Rongyun et al., 2020].

Table 1. The pseudocode scheme of the EKF algorithm.

Initialization Step:

$x_0(\mu_0, P_0)$, an initial error covariance matrix

Estimation Step:

$\bar{x}_k = f\left(\hat{x}_{k-1}\right)\quad or\quad \bar{x}_k = x_{k-1} + f\left(x_{k-1}\right)T_s$

$\bar{P}_k = J_f\left(\hat{x}_{k-1}\right)P_{k-1}{J_f}^T\left(x_{k-1}\right)+Q_{k-1}$

or

$\bar{P}_k = P_{k-1}+\left[J_f\left(\hat{x}_{k-1}\right)P_{k-1}+P_{k-1}{J_f}^T\left(x_{k-1}\right)\right]T_s+Q_{k-1}$

Update Step:

$\hat{x}_k = \bar{x}_k + K_k\left(z_k - h\left(\bar{x}_k\right)\right)$

$K_k = \bar{P}_k\,{J_h}^T\left(\bar{x}_k\right)\left[J_h\left(\bar{x}_k\right)\bar{P}_k{J_h}^T\left(\bar{x}_k\right)+R_k\right]^{-1}$

$P_k = \left[I - K_k J_h\left(\bar{x}_k\right)\right]\bar{P}_k$

where values written with "^" represent optimal estimations. The optimal gain that makes the best prediction is known as the Kalman gain (K_k). $J_f(.)$, $J_h(.)$ are the linear Jacobian matrices of nonlinear equations of state matrices ($f(.), h(.)$), respectively. If the state equations are linear, the Jacobian matrices are written as follows in Eq.27

$$
\begin{aligned}
&x_k = \underbrace{A x_{k-1} + B u_{k-1}}_{f(x_{k-1})} + w_{k-1} \quad \rightarrow \quad J_f\left(\hat{x}_{k-1}\right) = A\\
&z_k = \underbrace{C x_k}_{h(x_k)} + v_k \qquad\qquad\quad \rightarrow \quad J_h\left(\bar{x}_k\right) = C
\end{aligned}
\tag{27}
$$

4.1. Application of EKF Algorithm to IPMSM

The dynamic equations of IPMSM in the $\alpha-\beta$ axis set are as in Eq.28 [Nordin et al., 2021].

Preprints (www.preprints.org) | NOT PEER-REVIEWED | Posted: 20 October 2022 doi:10.20944/preprints202210.0298.v1

$$\frac{di_{\alpha s}}{dt} = -\frac{R_s}{L_s} i_{\alpha s} + \frac{\omega_m \psi_m}{L_s} \sin\theta_m + \frac{V_{\alpha s}}{L_s}$$
$$\frac{di_{\beta s}}{dt} = -\frac{R_s}{L_s} i_{\alpha s} - \frac{\omega_m \psi_m}{L_s} \cos\theta_m + \frac{V_{\beta s}}{L_s} \quad (28)$$
$$\frac{d\theta_m}{dt} = \omega_m$$

If the state variables of the machine state space model are selected as $x = \begin{bmatrix} i_{\alpha s} & i_{\beta s} & \omega_m & \theta_m \end{bmatrix}^T$ the EKF equations are stated in Eq.29.

$$f\left(x(t)\right) = \begin{bmatrix} f_1 \\ f_2 \\ f_3 \\ f_4 \end{bmatrix} = \begin{bmatrix} -\frac{R_s}{L_s} i_{\alpha s} + \frac{\omega_m \psi_m}{L_s} \sin\theta_m + \frac{V_{\alpha s}}{L_s} \\ -\frac{R_s}{L_s} i_{\alpha s} - \frac{\omega_m \psi_m}{L_s} \cos\theta_m + \frac{V_{\beta s}}{L_s} \\ 0 \\ \omega_m \end{bmatrix}$$
$$z = \begin{bmatrix} i_{\alpha s} & i_{\beta s} \end{bmatrix}^T$$
$$x_k = f\left(x_{k-1}\right) + w_{k-1}$$
$$z_k = C\, x_k + v_k$$
$$J_f = \left.\frac{\partial f}{\partial x}\right|_{x=x(t)} = \begin{bmatrix} -\frac{R_s}{L_s} & 0 & \frac{\psi_m}{L_s}\sin\theta_m & \frac{\omega_m \psi_m}{L_s}\cos\theta_m \\ 0 & -\frac{R_s}{L_s} & -\frac{\psi_m}{L_s}\sin\theta_m & \frac{\omega_m \psi_m}{L_s}\sin\theta_m \\ 0 & 0 & 0 & 0 \\ 0 & 0 & 1 & 0 \end{bmatrix} \quad (29)$$

An important point in EKF design is the determination of covariance matrices, which is often done by trial and error. A sensorless backstepping control block diagram of EKF-based IPMSM is demonstrated in Fig.3.

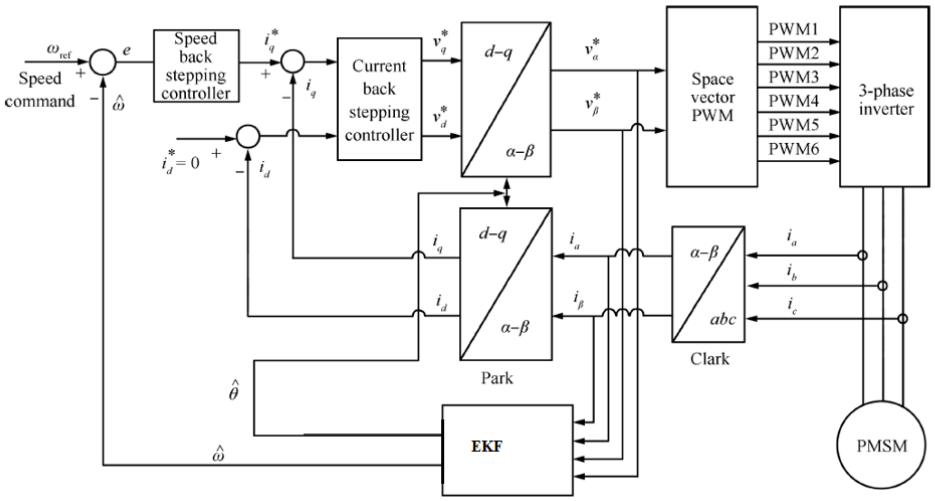

Figure 3. Sensorless backstepping control block diagram of EKF-based IPMSM.

Preprints (www.preprints.org) | NOT PEER-REVIEWED | Posted: 20 October 2022 doi:10.20944/preprints202210.0298.v1

5. Simulation Results

The simulations were conducted using Matlab/Simulink program. EKF was implemented to estimate internal states in the model. The observer was designed with the requirements to have a higher bandwidth than the overall control loop. The EKF code was created via an s-function block and then put into the Simulink model. The parameters and the rated sizes of the motor used in the simulation are given in Table 2.

Table 2. Motor sizes and parameters used in the simulation.

Parameter	Value
Rated power	9 kW
Rated torque	20 Nm
Rated speed	4000 rev/min
R_s	2.48 Ω
$L_d = L_q$	14 mH
ψ_m	0.105 Vs/rad
p	2
J	0.02 kgm²
B	0.001 Nms/rad

A critical step in the construction of the EKF is the selection of the elements of the covariance matrices **Q** and **R**, as they will determine the performance, stability, and convergence. The large values of **Q** increase model noise and/or parameter uncertainties. Therefore the filter dynamics are getting fast, while steady-state performance is getting poorer. **R** matrix is associated with the measurement noise. Increasing the values of the elements in **R** leads to poorer transient response. The covariances are fixed for the simulations. The following values were selected:

$$P_0 = \begin{bmatrix} 0.01 & 0 & 0 & 0 & 0 \\ 0 & 0.01 & 0 & 0 & 0 \\ 0 & 0 & 0.01 & 0 & 0 \\ 0 & 0 & 0 & 0.01 & 0 \\ 0 & 0 & 0 & 0 & 10 \end{bmatrix}; Q = \begin{bmatrix} 0.4 & 0 & 0 & 0 & 0 \\ 0 & 0.004 & 0 & 0 & 0 \\ 0 & 0 & 200 & 0 & 0 \\ 0 & 0 & 0 & 2 & 0 \\ 0 & 0 & 0 & 0 & 0.01 \end{bmatrix}; R = \begin{bmatrix} 0.0374 & 0 \\ 0 & 0.0374 \end{bmatrix}$$

After various simulation experiments having different Q and R matrices, it was concluded that those values give a good transient response and steady-state performance. Fig.4 shows the simulation results of EKF state estimation performance and backstepping controller trajectory tracking performance for the sensorless IPMSM drive.

Preprints (www.preprints.org) | NOT PEER-REVIEWED | Posted: 20 October 2022 doi:10.20944/preprints202210.0298.v1

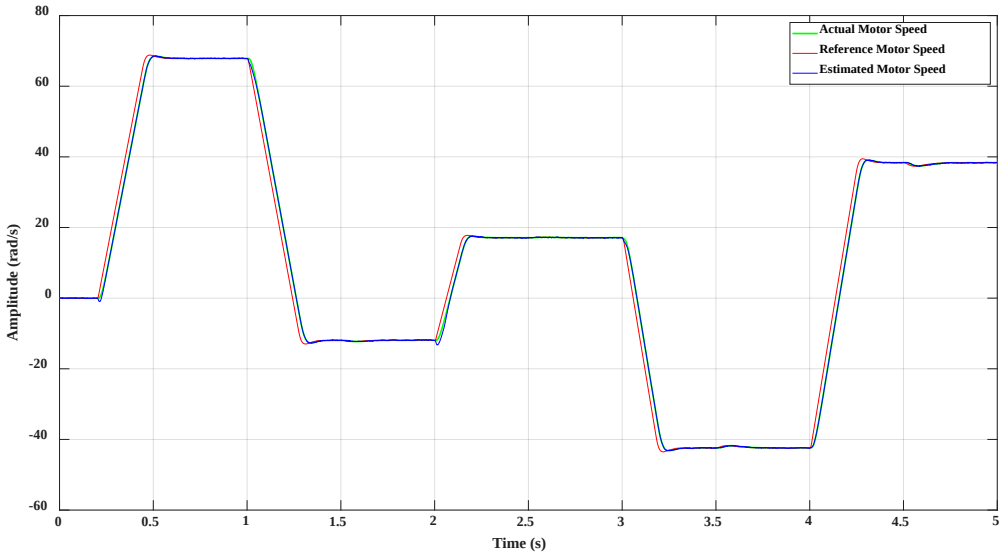

Figure 4. EKF estimation and backstepping controller performance: motor speed state for no-load speed variation and speed reversal.

It can be stated that EKF is capable of tracking the speed state satisfactorily under noisy machine operation. Besides, In Fig.5, the measured and estimated stator currents in the alpha-beta domain are demonstrated.

a)

Preprints (www.preprints.org) | NOT PEER-REVIEWED | Posted: 20 October 2022 doi:10.20944/preprints202210.0298.v1

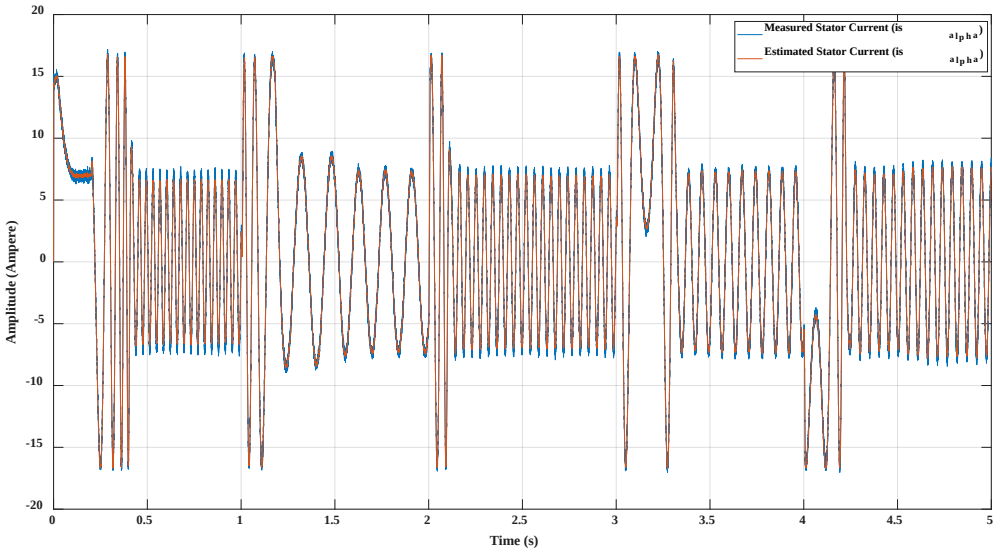

b)

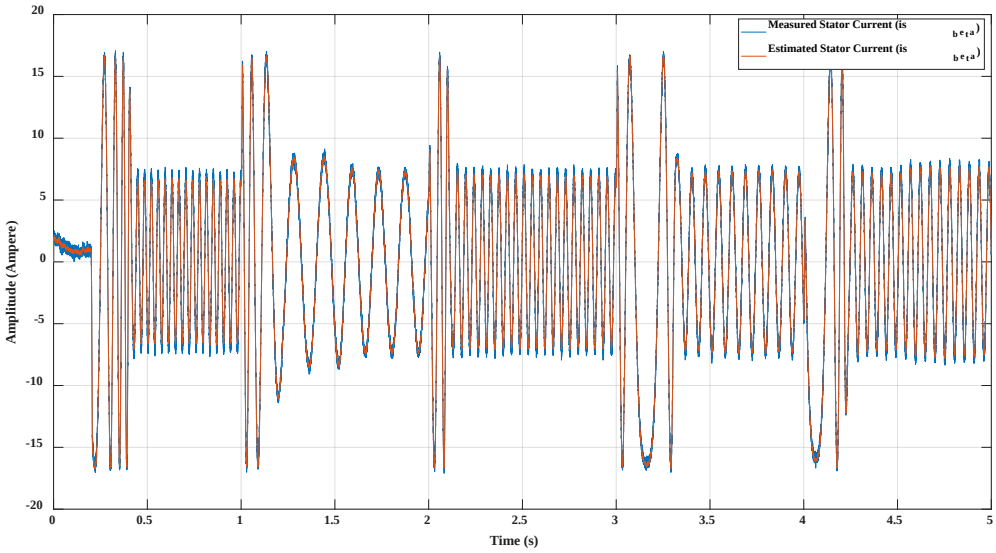

Figure 5. EKF performance: a) measured and estimated stator currents on α-axis, b) measured and estimated stator current on β-axis.

The control is affected by noisy measurements, it can be deduced that the achieved objective of FOC, the EKF gives good estimates of the speed with the rejection of noises, and the control response is improved. In another scenario, the simulation results are given when the reference speed is 400 rad/s and the motor is loaded with a step load of 20 Nm (rated torque) at t=3 s.

Fig.6 shows the backstepping control performance under the condition of the load torque variations.

Preprints (www.preprints.org) | NOT PEER-REVIEWED | Posted: 20 October 2022 doi:10.20944/preprints202210.0298.v1

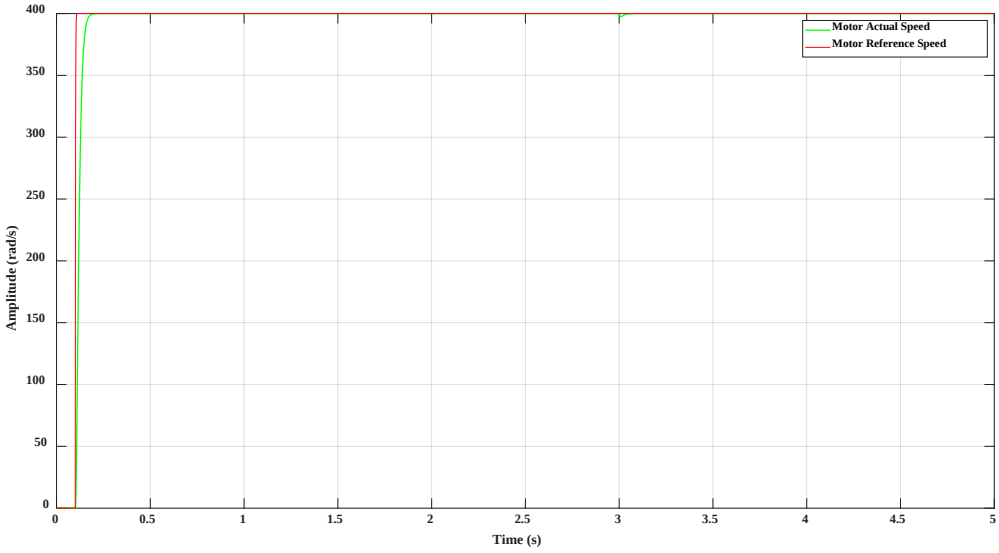

Figure 6. Backstepping control performance: motor speed state under load torque variation.

In Fig.7, the time-dependent variation of stator currents in the direct and quadrature axis is presented.

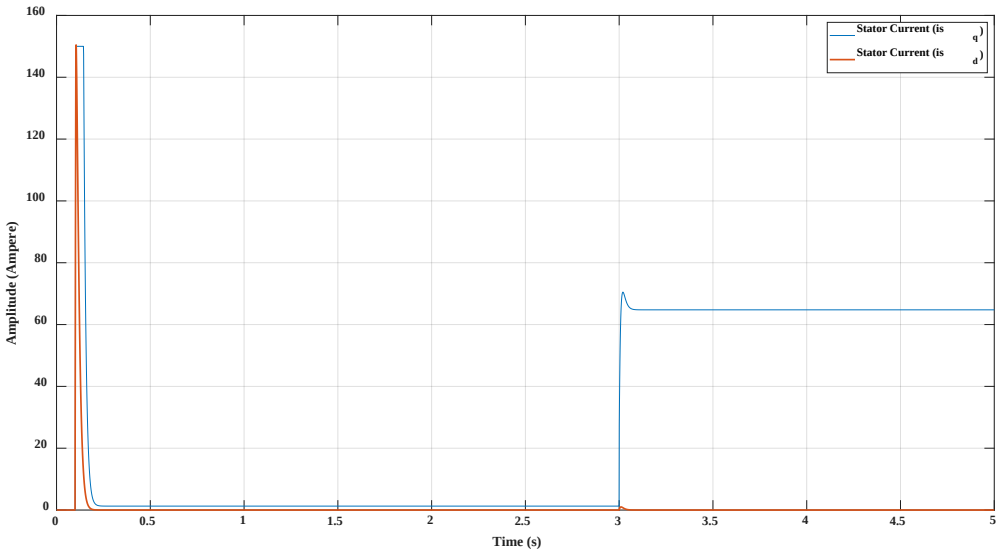

Figure 7: Time-dependent variation of stator currents in direct and quadrature axis.

In Fig.8, the time-dependent variation of motor torque and load torque is demonstrated. The current components of the direct and quadrature axis behave decoupled. The direct axis current is always forced to zero to orient all the linkage flux in the d-axis and achieve maximum torque per ampere.

Preprints (www.preprints.org) | NOT PEER-REVIEWED | Posted: 20 October 2022 doi:10.20944/preprints202210.0298.v1

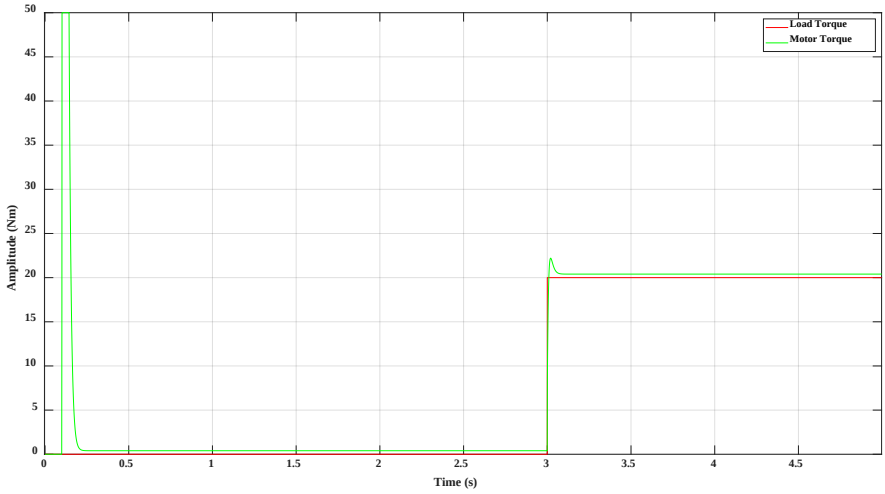

Figure 8: The time-dependent variation of motor torque and load torque.

The results show the effectiveness and fast response without overshoot at tracking a reference speed under parameter and load torque variations throughout the system.

6. Conclusion

The simulation results indicate that EKF is capable of tracking the actual rotor speed and that the elements of the covariance matrices, which are extracted via a trial-and-error process, are properly chosen. The transient response, steady-state performance, and robustness against the noise of the EKF seem satisfactory under the condition of the variable load and speed cases and process uncertainties. EKF is a good choice as the algorithms and models are easier to optimize for real-time implementation, high performance, and low cost for the microprocessors. The simulation results related to the backstepping controller demonstrate excellent speed tracking and anti-disturbance performance while ensuring the asymptotical stability of the system over a large span of operating conditions. The overall methodology gives a significant enhancement in performance and stability. The backstepping technique combined with vector control provides high control performance and robustness Moreover, the elimination of the sensor reduces the constraints and gives more flexibility to control the IPMSM.

Funding Information: The author states no funding is involved.

Author contributions: The author accepted responsibility for the entire content of this manuscript and approved its submission

Conflict of interest: The author state no conflict of interest.

References

1. Aishwarya, V., & Jayanand, B. (2016). Estimation and control of sensorless brushless DC motor drive using extended Kalman filter. 2016 International Conference on Circuit, Power and Computing Technologies (ICCPCT).
2. Aite Driss, Y., & Yousfi, D. (2013). PMSM sensorless control using back-emf based position and speed estimation method. 2013 International Renewable and Sustainable Energy Conference (IRSEC).
3. Anping, Z., & Jian, W. (2010). Observation method for PMSM rotor position based on high frequency signal injection. 2010 International Conference on Electrical and Control Engineering.
4. Asri, A., Ishak, D., Iqbal, S., & Kamarol, M. (2011). A speed sensorless field oriented control of parallel- connected dual PMSM. 2011 IEEE International Conference on Control System, Computing and Engineering.
5. Aydeniz, M.G., & Şenol,İ. (2011). A Luenberger-sliding mode observer with rotor time constant parameter estimation in induction motor drives. Turkish Journal of Electrical Engineering and Computer Sciences.

6. Benchabane, F., Titaoui, A., Bennis, O., Yahia, K., & Taibi, D. (2010). Systematic fuzzy sliding mode approach combined with extented Kalman filter for permanent magnet synchronous motor control. 2010 IEEE International Conference on Systems, Man and Cybernetics.
7. Benjak, O., & Gerling, D. (2010). Review of position estimation methods for IPMSM drives without a position Sensor Part II: Adaptive methods. The XIX International Conference on Electrical Machines - ICEM 2010.
8. Benjak, O., & Gerling, D. (2010a). Review of position estimation methods for IPMSM drives without a position sensor part I: Nonadaptive methods. The XIX International Conference on Electrical Machines - ICEM 2010.
9. Benjak, O., & Gerling, D. (2010b). Review of position estimation methods for IPMSM drives without a position Sensor Part II: Adaptive methods. The XIX International Conference on Electrical Machines - ICEM 2010.
10. Bernard, N., Dang, L., Olivier, J. C., Bracikowski, N., Wasselynck, G., & Berthiau, G. (2015). Design optimization of high-speed PMSM for electric vehicles. 2015 IEEE Vehicle Power and Propulsion Conference (VPPC).
11. Boldea, I., & Agarlita, S. C. (2011). The active flux concept for motion-sensorless unified AC Drives: A Review. International Aegean Conference on Electrical Machines and Power Electronics and Electromotion, Joint Conference.
12. Boldea, I., Paicu, M. C., Andreescu, G.-D., & Blaabjerg, F. (2009). "active flux" DTFC-SVM sensorless control of IPMSM. IEEE Transactions on Energy Conversion, 24(2), 314–322.
13. Bolognani, S., Oboe, R., & Zigliotto, M. (1999). Sensorless full-digital PMSM drive with EKF estimation of speed and rotor position. IEEE Transactions on Industrial Electronics, 46(1), 184–191.
14. Bolognani, S., Oboe, R., & Zigliotto, M. (1999). Sensorless full-digital PMSM drive with EKF estimation of speed and rotor position. IEEE Transactions on Industrial Electronics, 46(1), 184–191.
15. Brando, G., Cervone, A., Del Pizzo, A., & Spina, I. (2017). Sensorless control of single-inverter dual-motor AC brushless drives. 2017 IEEE International Symposium on Sensorless Control for Electrical Drives (SLED).
16. Butt, C., Hoque, M. A., & Rahman, M. A. (2003). Simplified fuzzy logic based MTPA speed control of IPMSM Drive. 38th IAS Annual Meeting on Conference Record of the Industry Applications Conference, 2003.
17. Chaoui, H., Gueaieb, W., & Yagoub, M. C. E. (2009). Neural network based speed observer for interior permanent magnet synchronous motor drives. 2009 IEEE Electrical Power & Energy Conference (EPEC).
18. Comnac, Cirstea, Moldoveanu, Ilea, & Cernat. (2002). Sensorless speed and direct torque control of interior permanent magnet synchronous machine based on extended Kalman filter. Proceedings of the IEEE International Symposium on Industrial Electronics ISIE-02.
19. Corley, M. J., & Lorenz, R. D. (1998). Rotor position and velocity estimation for a salient-pole permanent magnet synchronous machine at standstill and high speeds. IEEE Transactions on Industry Applications, 34(4), 784–789.
20. De Belie, F. M. L., Sergeant, P., & Melkebeek, J. A. (2010). A sensorless drive by applying test pulses without affecting the average-current samples. IEEE Transactions on Power Electronics, 25(4), 875–888. https://doi.org/10.1109/tpel.2009.2036617
21. De Soricellis, M., & Rapp, H. (2019). Current and voltage shaping method via modified d – q transformation for the torque ripple compensation in PMSMs. The Journal of Engineering, 2019(17), 3812–3817.
22. Devgan, S. K. (1988). Permanent magnet synchronous motors. University of Manchester Institute of Science and Technology (UMIST).
23. Dhaouadi, R., Mohan, N., & Norum, L. (1991). Design and implementation of an extended Kalman filter for the state estimation of a permanent magnet synchronous motor. IEEE Transactions on Power Electronics, 6(3), 491–497.
24. Dilys, J., Stankevič, V., & Łuksza, K. (2021). Implementation of extended Kalman filter with optimized execution time for sensorless control of a PMSM using ARM cortex-M3 microcontroller. Energies, 14(12), 3491.
25. Dobrucky, B., Michalik, J., Spanik, P., & Bobek, V. (2006). Virtual HF injection method (VHFIM) of rotor position estimation of PMSM under Field Oriented Control. International Symposium on Power Electronics, Electrical Drives, Automation and Motion, 2006. SPEEDAM 2006.
26. Elmas, Ç., & Zelaya-De La Parra, H. (1996). Application of a full-order Extended Luenberger Observer for a position sensorless operation of a switched reluctance motor drive. IEE Proceedings - Control Theory and Applications, 143(5), 401–408.
27. Engelmann, R. H., & Middendorf, W. H. (1995). Handbook of Electric Motors. M. Dekker.
28. Febin Daya, J. L., & Subbiah, V. (2010). Robust control of sensorless permanent magnet synchronous motor drive using Fuzzy Logic. 2010 2nd International Conference on Advanced Computer Control.
29. Gamazo-Real, J. C., Vázquez-Sánchez, E., & Gómez-Gil, J. (2010). Position and speed control of brushless DC motors using sensorless techniques and application trends. Sensors, 10(7), 6901–6947.
30. Gra˘dinaru Vlad-Nicolae. (2012). High Speed Brushless Dc Pmsm: Optimal Design and control contributions. Politehnica.
31. Haque, M. E., & Rahman, M. F. (2009). Permanent magnet synchronous motor drives: Analysis, modeling and Control. VDM Verlag Dr. Mu¨ller.
32. Haykin, S. S. (2001). Kalman filtering and Neural Networks. Wiley.
33. Honglin Zhou, Mingwei Kuang, & Jiandong Wu. (2012). A rotor position and speed estimation method for sensorless control of permanent magnetic synchronous motor. 2012 3rd IEEE International Symposium on Power Electronics for Distributed Generation Systems (PEDG).

34. Hughes, A. (2006). Electric motors and drives: Fundamentals, types, and applications. Elsevier/Newnes.
35. Ichikawa, S., Zhiqian Chen, Tomita, M., Doki, S., & Okuma, S. (2001). Sensorless control of an interior permanent magnet synchronous motor on the rotating coordinate using an extended electromotive force. IECON'01. 27th Annual Conference of the IEEE Industrial Electronics Society (Cat. No.37243).
36. Iqbal, M. A., & Memon, A. Y. (2019). Robust backstepping sensorless speed control of PMSM using cascaded sliding mode and high gain observers. 2019 International Symposium on Recent Advances in Electrical Engineering (RAEE).
37. Janiszewski, D. (2010). Extended Kalman filter based speed sensorless PMSM control with load reconstruction. Kalman Filter.
38. Jiaxi, L., Guijie, Y., & Pengfei, Y. (2007). Rotor position estimation for PMSM based on Sliding mode observer. 2007 International Conference on Mechatronics and Automation.
39. Jung-Hyo Lee, T.ae-Woong Kong, Won-Cheol Lee, Chung -Yuen Won, & Jae-Sung Yu. (2008). A new hybrid sensorless method using a back EMF estimator and a current model of permanent magnet synchronous motor. 2008 IEEE Power Electronics Specialists Conference.
40. Kim, P., & Huh, L. (2011). Kalman filter for beginners: With Matlab examples. CreateSpace.
41. Kim, T., Lee, H.-W., & Ehsani, M. (2007). Position sensorless brushless DC Motor/generator drives: Review and future trends. IET Electric Power Applications, 1(4), 557.
42. Kim, T.-H., & Ehsani, M. (2004). Sensorless control of the BLDC Motors from near-zero to high speeds. IEEE Transactions on Power Electronics, 19(6), 1635–1645.
43. Krishnan, R. (2017). Rotor position estimation and position sensorless control. Permanent Magnet Synchronous and Brushless DC Motor Drives, 423–454.
44. Laskaris, K. I., & Kladas, A. G. (2008). High torque internal permanent magnet wheel motor for electric traction applications. 2008 18th International Conference on Electrical Machines.
45. Lin, F.-J., Chen, S.-G., & Sun, I.-F. (2017). Adaptive backstepping control of six-phase PMSM using functional link radial basis function network uncertainty observer. Asian Journal of Control, 19(6), 2255–2269.
46. Louis, J.-P. (2011). Control of Synchronous Motors. ISTE/John Wiley&Sons.
47. Medagam, P. V., Yucelen, T., & Pourboghrat, F. (2009). Adaptive SDRE based nonlinear sensorless speed control for PMSM drives. 2009 American Control Conference.
48. Merzoug. (2011). Speed estimation using extended filter Kalman for the direct torque controlled Permanent Magnet Synchronous Motor (PMSM). Advances in Motor Torque Control.
49. Mohsin, O. (2000). Mobile robot localization based on Kalman filter. https://doi.org/10.15760/etd.1528
50. Nordin, M. I., Mat Lazi, J., Talib, M. H., & Ibrahim, Z. (2021). Speed sensorless control for PMSM drives using extended Kalman filter. Jurnal Teknologi, 84(1), 77–83.
51. Park, N.-S., Jang, M.-H., Lee, J.-S., Hong, K.-S., & Kim, J.-M. (2010). Performance improvement of a PMSM sensorless control algorithm using a stator resistance error compensator in the low speed region. Journal of Power Electronics, 10(5), 485–490.
52. Qiu, M. (2021). Extended Kalman filter application in permanent magnet synchronous motor sensorless control.
53. Rkhissi-Kammoun, Y., Ghommam, J., Boukhnifer, M., & Mnif, F. (2015). Rise-backsteppping feedback control for induction machine in Electric Vehicle Applications. 2015 23rd Mediterranean Conference on Control and Automation (MED).
54. Rongyun, Z., Changfu, G., Peicheng, S., Linfeng, Z., Changsheng, Z., & Chen, W. (2020). The permanent magnet synchronous motor sensorless control of electric power steering based on iterative fifth-order Cubature Kalman filter. Journal of Dynamic Systems, Measurement, and Control, 142(8).
55. Sagar, S. V., & Joseph, K. D. (2013). Speed estimation algorithms for sensorless control of PMSM. 2013 International Mutli-Conference on Automation, Computing, Communication, Control and Compressed Sensing (iMac4s).
56. Sain, C., Banerjee, A., Biswas, P. K., Thanikanti, S. B., & Baladhanautham, C. B. (2021). Sensor angle-based control strategy and dynamic analysis of a sinusoidal pulse width modulation-operated permanent Magnet Synchronous Machine Drive for Electric Propulsion Unit. International Transactions on Electrical Energy Systems, 31(12).
57. Shanshan Wu, Yongdong Li, & Xuejin Miao. (2007). Comparison of signal injection methods for sensorless control of PMSM at very low speeds. 2007 European Conference on Power Electronics and Applications.
58. Shen, J. X., Zhu, Z. Q., & Howe, D. (2003). Sensorless flux-weakening control of permanent magnet brushless machines using third-harmonic back-EMF. IEEE International Electric Machines and Drives Conference, 2003. IEMDC'03.
59. Shibano, Y., & Kubota, H. (2009). Pole position estimation method of IPMSM at low speed without high frequency components injection. 2009 Twenty-Fourth Annual IEEE Applied Power Electronics Conference and Exposition.
60. Song, Z., Yao, W., & Lee, K. (2021). High-precision sensorless control method with fast dynamic response for high-speed PMSM based on discrete-time back-EMF deadbeat observer. 2021 IEEE Energy Conversion Congress and Exposition (ECCE).
61. Tanaka, K., & Miki, I. (2007). Position sensorless control of interior permanent magnet synchronous motor using extended electromotive force. Electrical Engineering in Japan, 161(3), 41–48.
62. Toso, F., Carlet, P. G., Preindl, M., & Bolognani, S. (2018). Active-flux-based motion-sensorless control of PMSM using moving horizon estimator. 2018 IEEE 9th International Symposium on Sensorless Control for Electrical Drives (SLED).

63. Urbanski, K., & Janiszewski, D. (2021). Position estimation at zero speed for PMSMs using artificial neural networks. Energies, 14(23), 8134.
64. Vyncke, T. J., Boel, R. K., & Melkebeek, J. A. (2010). On extended Kalman filters with augmented state vectors for the stator flux estimation in spmsms. 2010 Twenty-Fifth Annual IEEE Applied Power Electronics Conference and Exposition (APEC).
65. Wang, G., Zhang, G., & Xu, D. (2019). Practical issues of sensorless control for PMSM drives. Position Sensorless Control Techniques for Permanent Magnet Synchronous Machine Drives, 281–295.
66. Wang, Y., Zhu, J., Guo, Y., Li, Y., & Xu, W. (2010). Torque ripples and estimation performance of high frequency signal injection based sensorless PMSM drive strategies. 2010 IEEE Energy Conversion Congress and Exposition.
67. Wei-Hua Li, Zi-Ying Chen, & Wen-Ping Cao. (2012). Simulation research on optimization of permanent magnet synchronous motor sensorless vector control based on Mras. 2012 International Conference on Wavelet Active Media Technology and Information Processing (ICWAMTIP).
68. Wu, J., Hu, Y., Zhang, B., Feng, G., & Liu, Z. (2022). Comparison and analysis of different rotor structures of double-stator permanent magnet synchronous motor. IET Electric Power Applications, 16(6), 685–700.
69. Xiao, D., Foo, G., & Rahman, M. F. (2010). A new combined adaptive flux observer with HF signal injection for sensorless direct torque and flux control of matrix converter fed IPMSM over a wide speed range. 2010 IEEE Energy Conversion Congress and Exposition.
70. Yamakawa, T., Wakao, S., Kondo, K., & Yoneyama, T. (2005). A new flux weakening operation of interior permanent magnet synchronous motors for Railway Vehicle Traction. 2005 European Conference on Power Electronics and Applications.
71. Ying Yan, & Jianguo Zhu. (2006). Simulation of a direct torque controlled PMSM drive incorporating structural and saturation saliencies. 37th IEEE Power Electronics Specialists Conference.
72. Yoon-Ho Kim, & Yoon-Sang Kook. (1999). High performance IPMSM drives without rotational position sensors using reduced-order EKF. IEEE Transactions on Energy Conversion, 14(4), 868–873.
73. Yousfi, D., Halelfadl, A., & El Kard, M. (2009). Review and evaluation of some position and speed estimation methods for PMSM sensorless drives. 2009 International Conference on Multimedia Computing and Systems.
74. Zhang, H., Chen, Z., & Zhang, H. (2021). Improved rotor position estimation for IPMSM drives in flux-weakening-based optimized synchronous modulation. 2021 24th International Conference on Electrical Machines and Systems (ICEMS).
75. Zhao, Y., Qiao, W., & Wu, L. (2013). An adaptive quasi-sliding-mode observer-based sensorless drive for heavy-duty interior permanent magnet synchronous machines. 2013 Twenty-Eighth Annual IEEE Applied Power Electronics Conference and Exposition (APEC).
76. Zhiqian Chen, Tomita, M., Doki, S., & Okuma, S. (2003). An extended electromotive force model for sensorless control of Interior Permanent-magnet synchronous motors. IEEE Transactions on Industrial Electronics, 50(2), 288–295.